JACS
JOURNAL OF THE AMERICAN CHEMICAL SOCIETY
Article
pubs.acs.org/JACS

# The Negative Ion Photoelectron Spectrum of *meta*-Benzoquinone Radical Anion ($MBQ^{\bullet-}$): A Joint Experimental and Computational Study

Bo Chen,[†] David A. Hrovat,[†] S. H. M. Deng,[‡] Jian Zhang,[‡,#] Xue-Bin Wang,*[,‡] and Weston Thatcher Borden*[,†]

[†]Department of Chemistry and the Center for Advanced, Scientific Computing and Modeling, University of North Texas, 1155 Union Circle, #305070, Denton, Texas 76203-5070, United States

[‡]Physical Sciences Division, Pacific Northwest National Laboratory, P.O. Box 999, MS K8-88, Richland, Washington 99352, United States

Supporting Information

**ABSTRACT:** Negative ion photoelectron (NIPE) spectra of the radical anion of *meta*-benzoquinone (**MBQ**, *m*-$OC_6H_4O$) have been obtained at 20 K, using both 355 and 266 nm lasers for electron photodetachment. The spectra show well-resolved peaks and complex spectral patterns. The electron affinity of **MBQ** is determined from the first resolved peak to be 2.875 ± 0.010 eV. Single-point, CASPT2/aug-cc-pVTZ//CASPT2/aug-cc-pVDZ calculations predict accurately the positions of the 0−0 bands in the NIPE spectrum for formation of the four lowest electronic states of neutral **MBQ** from the $^2A_2$ state of $MBQ^{\bullet-}$. In addition, the Franck−Condon factors that are computed from the CASPT2/aug-cc-pVDZ optimized geometries, vibrational frequencies, and normal mode vectors, successfully simulate the intensities and frequencies of the vibrational peaks in the NIPE spectrum that are associated with each of these electronic states. The successful simulation of the NIPE spectrum of $MBQ^{\bullet-}$ allows the assignment of $^3B_2$ as the ground state of **MBQ**, followed by the $^1B_2$ and $^1A_1$ electronic states, respectively 9.0 ± 0.2 and 16.6 ± 0.2 kcal/mol higher in energy than the triplet. These experimental energy differences are in good agreement with the calculated values of 9.7 and 15.7 kcal/mol. The relative energies of these two singlet states in **MBQ** confirm the previous prediction that their relative energies would be reversed from those in *meta*-benzoquinodimethane (**MBQDM**, *m*-$CH_2C_6H_4CH_2$).

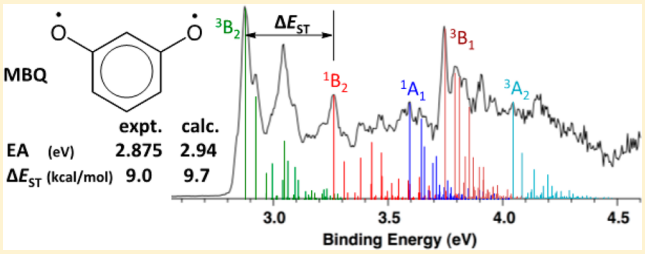


## INTRODUCTION

*meta*-Benzoquinodimethane (**MBQDM**) is a non-Kekulé hydrocarbon diradical in which the two nonbonding MOs have atoms in common. Because these two MOs are nondisjoint, qualitative theory predicts that the ground state of **MBQDM** is a triplet.[1] Quantitative electronic-structure calculations have, indeed, found the triplet to be the ground state of **MBQDM**,[2] and electron paramagnetic resonance (EPR) spectroscopy[3] and negative ion photoelectron spectroscopy (NIPES)[4] have both confirmed experimentally that the ground state of **MBQDM** is, in fact, a triplet.

As shown schematically in Figure 1, CASPT2/6-31G(d) calculations also predicted that the lowest singlet state of **MBQDM** is the $^1A_1$ state, which was computed to be 11.0 kcal/mol higher in energy than the $^3B_2$ ground state, but 11.9 kcal/mol lower than the $^1B_2$ state.[2c] The NIPE spectrum of $MBQDM^{\bullet-}$ gave values of the singlet−triplet energy difference in **MBQDM** of $\Delta E_{ST}$ = 9.6 ± 0.2 and <21.5 kcal/mol for the $^1A_1$ and $^1B_2$ states, respectively,[4] in reasonable agreement with the predicted energy differences between these three electronic states of **MBQDM**.

The reason why $^1A_1$ is both calculated and found to be substantially lower in energy than $^1B_2$ is easy to understand from the depictions of these two states of **MBQDM** in Figure 1.[2c] In the $^1A_1$ state the two nonbonding electrons are largely localized on the exocyclic methylene groups, leaving the six-membered ring with an aromatic, benzenoid, $\pi$ system. In contrast, in the $^1B_2$ state there is substantial $\pi$ bonding to the exocyclic methylene groups, at the expense of the aromaticity of the $\pi$ system of the six-membered ring in **MBQDM**.

Calculations have also been performed on *meta*-benzoquinone (**MBQ**),[2c,5] but much less is known experimentally about this dioxa derivative of **MBQDM**, than about the hydrocarbon.[6] Multireference CI[5a] and CASPT2 calculations[2c] both predict a reversal in the ordering of the two lowest singlet states on going from **MBQDM** to **MBQ**. At the CASPT2/6-31G(d) level of theory, the lowest singlet state of **MBQ** is predicted to be the $^1B_2$ state, which is calculated to be 11.9 kcal/mol higher in energy than the $^3B_2$ ground state but 11.0 kcal/mol lower than

Received: December 6, 2013
Published: February 19, 2014

   dx.doi.org/10.1021/ja412433t | J. Am. Chem. Soc. 2014, 136, 3589−3596

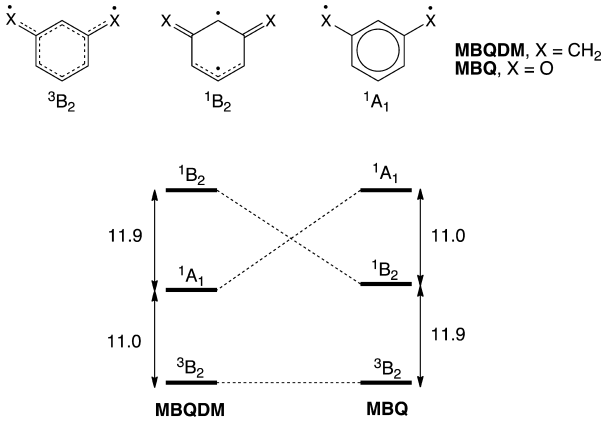


**Figure 1.** Schematic depiction of the bonding and the CASPT2/6-31G(d) relative energies of the three lowest electronic states of **MBQDM** and **MBQ**.[2c]

the $^1A_1$ state. This predicted reversal in the ordering of the two lowest singlet states between **MBQDM** and **MBQ** is shown schematically in Figure 1.

The reason for the predicted change in the ordering of the two lowest singlet states of **MBQDM** and **MBQ** is also apparent from the depictions of the bonding in these states in Figure 1.[2c,5a] Since C═O $\pi$ bonding is much more favorable energetically than C═C $\pi$ bonding, the strong $\pi$ bonding to the exocyclic atoms, X, in the $^1B_2$ state is much more favorable for X = O in **MBQ** than for X = $CH_2$ in **MBQDM**. According to the CASPT2/6-31G(d) results, the change from X = $CH_2$ to X = O results in a 23 kcal/mol predicted change in the relative energies of the $^1A_1$ and $^1B_2$ states on going from **MBQDM** to **MBQ**.

This prediction could, in principle, be tested by obtaining and analyzing the NIPE spectrum of the **MBQ** radical anion (**MBQ**$^{\bullet-}$). **MBQ**$^{\bullet-}$ was first generated in 2005,[7] but its NIPE spectrum was not reported until 2011.[8] Unfortunately, the NIPE spectrum was not well resolved, and unequivocal assignments of the peaks in it could not be made.

We have now been able to obtain a much better-resolved NIPE spectrum of **MBQ**$^{\bullet-}$. In order to analyze this spectrum, we have carried out calculations of the energies of each of the seven, low-lying electronic states of **MBQ** that can be formed by detachment of an electron from the radical anion. In addition, we have computed the intensities and spacings of the peaks in the vibrational progressions for formation of each of these electronic states of **MBQ** by photodetachment of an electron from **MBQ**$^{\bullet-}$.

Herein, we report the well-resolved NIPE spectrum of **MBQ**$^{\bullet-}$ and describe the successful simulation of the spectrum and the assignments of the electronic states of **MBQ** that are based on these simulations. Our analysis of the NIPE spectrum of **MBQ**$^{\bullet-}$ confirms the predicted reversal of the energies of the two lowest singlet states on going from **MBQDM** to **MBQ**.[2c,5a]

## NIPE SPECTROSCOPY OF MBQ$^{\bullet-}$

Well-resolved NIPE spectra were obtained by combining electrospray generation of **MBQ**$^{\bullet-}$ in the gas-phase with a temperature-controlled ion trap and a magnetic bottle, time-of-flight, photoelectron spectrometer that was recently developed at PNNL.[9] An anhydrous 0.1 mM methanolic solution of resorcinol, titrated with a small amount of NaOH dissolved in methanol, was prepared in a $N_2$ glovebox, and used to generate **MBQ**$^{\bullet-}$ by electrospray under an atmosphere of $N_2$. The anions produced were guided by two RF-only quadrupoles and directed by a 90° ion bender to the temperature-controlled, cryogenic, ion trap cooled to $T$ = 20 K. There, the ions were accumulated and cooled for 20−100 ms, via collisions with a buffer gas of 0.1 mTorr helium, containing 20% $H_2$, before being pulsed out into the extraction zone of a time-of-flight mass spectrometer with a repetition rate of 10 Hz.

During each NIPES experiment, the **MBQ**$^{\bullet-}$ was mass-selected and maximally decelerated before being intercepted by a probe laser beam in the photodetachment zone. In the current study, photon energies of 266 nm (4.661 eV) and 355 nm (3.496 eV), both from a Nd:YAG laser, were used. The laser was operated at a 20 Hz repetition rate, with the ion beam off at alternating laser shots, thus allowing for shot-by-shot background-subtracted spectra to be obtained. Photoelectrons were collected at nearly 100% efficiency by a magnetic bottle and analyzed in a 5.2 m long electron flight tube.

Time-of-flight photoelectron spectra were collected and converted to kinetic energy spectra, with calibration furnished by the known spectra of $I^-$ and $ClO_2^-$. The electron binding energy spectra, presented in this paper, were obtained by subtracting the kinetic energy spectra from the photon energies. The energy resolution ($\Delta E$/kinetic energy) was about 2%, that is, ∼20 meV full width at half-maximum for 1 eV electrons, as estimated from the NIPE spectrum of $I^-$ at 355 nm.

## COMPUTATIONAL METHODOLOGY

The $C_{2v}$ geometries of the two low-lying states of **MBQ**$^{\bullet-}$ were initially optimized, using (9/8)CASSCF calculations; and the geometries of the triplet and two low-lying singlet states of neutral **MBQ** were initially optimized at the (8/8)CASSCF level. All of the $\pi$ electrons, distributed among three bonding, two nonbonding, and three antibonding $\pi$ MOs, were included in the active spaces for these CASSCF calculations. An aug-cc-pVDZ basis set[10] was used for the geometry optimizations.

The (8/8)CASSCF optimized geometry for the $^1A_1$ state has C−O bond lengths that seemed unusually long (1.321 Å). CASSCF calculations tend to overemphasize the avoidance of ionic terms in wave functions;[11] and it seemed possible that our (8/8)CASSCF calculation on the $^1A_1$ state of **MBQ** was providing too much localization of the nonbonding electrons in the 2p-$\pi$ MOs of the oxygens. Therefore, we reoptimized the geometry of the $^1A_1$ state of **MBQ**, with inclusion of dynamic electron correlation,[11] at the (8/8)CASPT2 level of theory.[12]

In fact, the (8/8)CASPT2 optimized geometry for the $^1A_1$ state has C−O bond lengths that are 0.057 Å shorter than those in the (8/8)CASSCF optimized geometry. The coefficients of the two major configurations in the $^1A_1$ state of **MBQ**, $|...3b_1^2\rangle$ and $|...2a_2^2\rangle$, change from, respectively, 0.71 and −0.59 at the (8/8)CASSCF optimized geometry to 0.86 and −0.37 at the (8/8)CASPT2 optimized geometry. The increase in the weight of the dominant configuration on going from the (8/8)CASSCF to the (8/8)CASPT2 optimized geometry shows that the diradical character in the wave function for the $^1A_1$ state decreases in going from the former to the latter geometry. Therefore, the schematic depiction in Figure 1 of $^1A_1$ as a diradical is more descriptive of the (8/8)CASSCF optimized geometry than of the (8/8)CASPT2 optimized geometry.

A population analysis of the (8/8)CASPT2/aug-cc-pVTZ wave function at the (8/8)CASPT2/auc-cc-pVDZ optimized geometry (see Table S-4 of the Supporting Information [SI]), indicates that the $^1A_1$ state of **MBQ** can be better described as being a 1,3-propanedion-2-yl anion, joined by a pair of C−C ring bonds to an allylic cation. As also shown in Table S-4 of the SI, the B3LYP/aug-cc-pVTZ optimized geometry of $^1A_1$ is similar to that obtained by the (8/8)CASPT2 geometry optimization, and a population analysis of the B3LYP wave function is also consistent with the depiction of the $^1A_1$ state of **MBQ**


dx.doi.org/10.1021/ja412433t | J. Am. Chem. Soc. 2014, 136, 3589−3596

as having a large contribution from the zwitterionic structure that is shown in Scheme 1.

**Scheme 1**

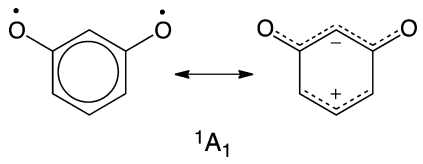


Most importantly, the (8/8)CASPT2/aug-cc-pVTZ energy of $^1A_1$ is 7.8 kcal/mol lower when the energy is computed at the (8/8)CASPT2/aug-cc-pVDZ optimized geometry, rather than at the (8/8)CASSCF/aug-cc-pVDZ optimized geometry. This finding demonstrates again[11] that, because CASSCF optimized geometries can be quite different from the optimized geometries that are obtained when dynamic electron correlation is included in the electronic wave functions, CASPT2 single-point energies, computed at CASSCF optimized geometries, can give energies that are significantly in error.

For the sake of consistency, the geometries of **MBQ**$^{\bullet-}$ and of all of the low-lying, singlet and triplet states of **MBQ** were optimized at the CASPT2 level of theory, using the aug-cc-pVDZ[10] basis set. These geometry optimizations and subsequent CASPT2 single-point calculations with the aug-cc-pVTZ basis set[10] were carried out with MOLCAS 7.4.[13] The CASPT2 optimized geometries are given in Table 1 and in the SI for this study, where they are compared with B3LYP/aug-cc-pVTZ optimized geometries.

In addition to performing calculations on the triplet and two lowest-energy singlet states of **MBQ**, which each contain eight $\pi$ electrons, calculations were also performed on the two lowest-energy singlet and triplet states that each have nine $\pi$ electrons. These excited states can be formed by transferring an electron from a symmetry combination of the nonbonding 2p−$\sigma$ AOs on the two oxygens into the $\pi$ MOs. For these calculations the CASSCF and CASPT2 active space was expanded to 12 electrons in 10 orbitals, so that the nonbonding 2p−$\sigma$ AOs on the oxygens and the electrons in them were included in the active space.[14]

Vibrational analysis on each electronic state of **MBQ** was carried out at the CASPT2/aug-cc-pVDZ[10] level of theory, using finite energy differences. MOLCAS[13] allows CASPT2 frequencies to be computed for only totally symmetric displacements, which maintain the $C_{2v}$ symmetry of **MBQ**. Fortunately, for simulating NIPE spectra, only the frequencies of totally symmetric vibrations are needed.

In order to simulate the vibrational structure in the NIPE spectrum of **MBQ**$^{\bullet-}$, the optimized geometries, harmonic vibrational frequencies (unscaled), and normal mode vectors, obtained from the CASPT2/aug-cc-pVDZ calculations, were used as input to the ezSpectrum (version 3.0) program.[15] This program calculated the Franck−Condon factors (FCFs),[16] for electronic transitions from the optimized geometry of the lowest electronic state of the radical anion to each of the low-lying, electronic states of neutral **MBQ**. The calculated FCFs were then used to simulate the vibrational structure in the NIPE spectrum for formation of each electronic state of **MBQ**.

## RESULTS AND DISCUSSION

**The NIPE Spectra of MBQ**$^{\bullet-}$**.** The well-resolved NIPE spectra of **MBQ**$^{\bullet-}$, obtained with 355 nm and 266 nm lasers, are shown in Figure 2a and b, respectively. The 355 nm spectrum features a large peak, marked X, at an electron binding energy (EBE) of 2.875 ± 0.010 eV. It is followed by several well-resolved smaller peaks at EBEs between 2.90−3.20 eV, and they are followed by what appears to be the origin of a new band, marked A, at an EBE of 3.265 eV. Because the experiments were conducted at 20 K, no hot bands are expected to be present in the NIPE spectrum.

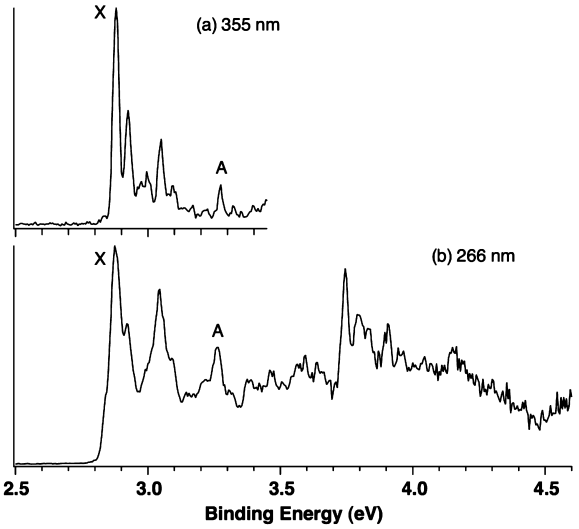


**Figure 2.** The low-temperature (20 K) NIPE spectra of **MBQ**$^{\bullet-}$ at (a) 355 and (b) 266 nm. The origins of the bands for what could be the first two electronic states of **MBQ** are marked X and A.

The higher intensity of band X than of band A suggests that band X belongs to a triplet, which has three spin components, and that band A belongs to a singlet, which has only one spin component.[1c,17] Therefore, the NIPE spectrum of MBQ$^{\bullet-}$ appears to confirm the prediction that, like **MBQDM**, **MBQ** has a triplet ground state.[2c,5a] However, the X − A energy difference of (3.265 − 2.875 = 0.390 eV) gives $\Delta E_{ST}$ = 9.0 kcal/mol, which is nearly 3 kcal/mol smaller than the predicted CASPT2/6-31G(d) energy difference between $^1B_2$ and $^3B_2$ of $\Delta E_{ST}$ = 11.9 kcal/mol in Figure 1.[2c]

**Table 1. Comparisons of the CASPT2/aug-cc-pVTZ//CASPT2/aug-cc-pVDZ Computed Electron Binding Energies (EBEs) with the Experimental EBEs of MBQ; CASPT2/aug-cc-pVDZ Optimized Geometries of the Low-Lying Electronic States of MBQ Are Also Given**

| electronic state | | $^2A_2$ | $^3B_2$ | $^1B_2$ | $^1A_1$ | $^3B_1$ | $^1B_1$ | $^1A_2$ | $^3A_2$ |
|---|---|---|---|---|---|---|---|---|---|
| calculated EBE kcal/mol (eV) | | | 67.7 (2.94) | 77.4 (3.36) | 83.4 (3.62) | 87.2 (3.78) | 87.8 (3.81) | 93.9 (4.07) | 94.3 (4.09) |
| experimental EBE (eV) | | | (2.875) | (3.265) | (3.595) | (3.745) | – | – | (4.04) |
| bond lengths in Å | C1−O | 1.281 | 1.257 | 1.238 | 1.264 | 1.273 | 1.279 | 1.304 | 1.301 |
| | C1−C2 | 1.427 | 1.457 | 1.477 | 1.417 | 1.425 | 1.424 | 1.422 | 1.423 |
| | C1−C6 | 1.481 | 1.465 | 1.485 | 1.495 | 1.465 | 1.460 | 1.439 | 1.440 |
| | C5−C6 | 1.402 | 1.403 | 1.404 | 1.397 | 1.401 | 1.401 | 1.403 | 1.403 |
| bond angles in deg | C2−C1−O | 125.5 | 121.0 | 121.4 | 128.2 | 120.7 | 120.3 | 120.5 | 120.7 |
| | C1−C2−C3 | 123.0 | 121.6 | 122.2 | 120.1 | 118.8 | 118.7 | 119.4 | 119.6 |
| | C4−C5−C6 | 119.4 | 121.7 | 122.4 | 115.4 | 120.1 | 120.4 | 121.4 | 121.5 |


dx.doi.org/10.1021/ja412433t | J. Am. Chem. Soc. 2014, 136, 3589−3596

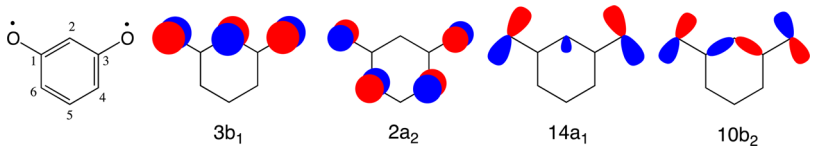


**Figure 3.** Schematic depiction of the two low-lying, nonbonding $\pi$ MOs of **MBQ** and of the two symmetry combinations of the 2p−$\sigma$ nonbonding lone-pair AOs on the oxygens.

The 266 nm NIPE spectrum has features similar to those of the 355 nm spectrum at EBEs between 2.85 and 3.27 eV; but, at higher EBEs, the 266 nm spectrum shows a complex series of peaks. The second highest peak in the 266 nm NIPE spectrum at 3.745 eV looks as though it could be the origin of the band for a third electronic state.

The complexity of the NIPE spectrum of **MBQ**$^{\bullet-}$ stands in sharp contrast to the simplicity of the NIPE spectrum of **MBQDM**$^{\bullet-}$, which shows three, well-separated bands, corresponding to the $^3B_2$ ground state, followed by the $^1A_1$ and $^1B_2$ singlet states.[4] The reason for this difference in complexity between the NIPE spectra of **MBQ**$^{\bullet-}$ and **MBQDM**$^{\bullet-}$ is that in **MBQ**$^{\bullet-}$ two lone pairs of electrons on each oxygen replace the C−H bonds in **MBQDM**$^{\bullet-}$. Since, in addition to photodetachment of one of the $\pi$ electrons, photodetachment of one of the oxygen lone-pair electrons can occur in **MBQ**$^{\bullet-}$, it is not surprising that the NIPE spectrum of **MBQ**$^{\bullet-}$ shows much more complexity than the NIPE spectrum of **MBQDM**$^{\bullet-}$.

The complexity of the NIPE spectrum of **MBQ**$^{\bullet-}$ makes it nearly impossible to assign the peaks in the spectrum without the aid of calculations. To make convincing assignments to the bands in the NIPE spectrum, not only the energies of the band origins but also the vibrational structure in the band for each electronic state should be reproduced by the calculations.

**Calculations on MBQ$^{\bullet-}$.** There are two low-lying electronic states of **MBQ**$^{\bullet-}$ that differ by which nonbonding $\pi$ MO, $3b_1$ or $2a_2$ in Figure 3, is singly occupied. Therefore, a successful analysis of the NIPE spectrum of **MBQ**$^{\bullet-}$ must begin with an identification of which of these two states is lower in energy.

Our CASPT2/aug-cc-pVTZ//CASPT2/aug-cc-pVDZ calculations find the $^2A_2$ state of **MBQ**$^{\bullet-}$, in which the $2a_2$ $\pi$ MO is singly occupied, to be lower in energy by 6.2 kcal/mol than the $^2B_1$ state, in which the $3b_1$ MO is singly occupied. As shown schematically in Figure 3, the $2a_2$ $\pi$ MO spans one more carbon than the $3b_1$ $\pi$ MO, so that the coefficients on the oxygens are smaller in $2a_2$ than in $3b_1$. Since oxygen is more electronegative than carbon, the $3b_1$ MO is lower in energy than the $2a_2$ MO. Therefore, the $^2A_2$ state of **MBQ**$^{\bullet-}$, in which the $3b_1$ MO is doubly occupied and the $2a_2$ $\pi$ MO is singly occupied, is lower in energy than the $^2B_1$ state, in which only one electron occupies the $3b_1$ MO and the $2a_2$ MO is doubly occupied.

**Calculations of the Energies of the Electronic States of MBQ.** In order to make provisional assignments of the position of the origin of each of the **MBQ** electronic states in the NIPE spectrum of **MBQ**$^{\bullet-}$, we performed CASPT2 calculations on neutral **MBQ**. The CASPT2/aug-cc-pVDZ optimized geometries and CASPT2/aug-cc-pVTZ energies of the seven lowest-lying electronic states of **MBQ** are given in Table 1.

Three of these states ($^3B_2$, $^1B_2$, and $^1A_1$) are formed by detaching one electron from either the $3b_1$ or $2a_2$ $\pi$ MO of the $^2A_2$ state of **MBQ**$^{\bullet-}$. At the CASPT2/aug-cc-pVTZ level, $^3B_2$ is computed to be the ground state of **MBQ**. The lowest singlet state is $^1B_2$, which is calculated to be 9.7 kcal/mol (0.42 eV) above the triplet ground state. The CASPT2 energy difference between these two electronic states of **MBQ** is lower by 2.2 kcal/mol when computed with the aug-cc-pVTZ basis set, rather than with the much smaller 6-31G(d) basis set.[2c]

Experimentally, the difference between peaks X and A in the NIPE spectra in Figure 2 is 9.0 kcal/mol (0.390 eV). The good agreement between the calculated $^1B_2 - {}^3B_2$ energy difference of 9.7 kcal/mol and the 9.0 kcal/mol energy difference between peaks X and A in the NIPE spectra, indicates that peak A probably is the onset of the $^1B_2$ state in the NIPE spectra.

The $^1A_1$ singlet state is calculated to be 6.0 kcal/mol (0.26 eV) higher in energy than the $^1B_2$ state and to have an EBE of 83.4 kcal/mol (3.62 eV). There is, in fact, a peak in the 266 nm NIPE spectrum in Figure 2, with an EBE of 3.595 eV, that has the highest intensity among a cluster of peaks extending from 3.35 to 3.70 eV. This peak could be provisionally assigned to the onset of the $^1A_1$ state. However, without additional evidence, it would be an act of faith in the accuracy of the CASPT2 calculations to make an unequivocal assignment of the peak at 3.595 eV to the onset of the $^1A_1$ state.

Detaching one electron in **MBQ**$^{\bullet-}$ from either the in-phase or out-of-phase combination of the oxygen 2p−$\sigma$ lone pair AOs, (respectively, MOs $14a_1$ and $10b_2$ in Figure 3), gives one unpaired $\sigma$ electron in **MBQ** and leaves nine electrons in the $\pi$ MOs. The unpaired $\sigma$ and the unpaired $\pi$ electrons can be coupled to form either a singlet or a triplet state.

Placing the unpaired $\sigma$ electron in the $14a_1$ MO and the unpaired $\pi$ electron in the $2a_2$ MO gives an electronic configuration of $A_2$ symmetry, as does placing the unpaired $\sigma$ electron in the $10b_2$ MO and the unpaired $\pi$ electron in the $3b_1$ MO. Since these two configurations have the same symmetry, they mix; and, since they also have nearly the same energy, they mix nearly equally. The lower energy combination that arises from this mixing is

$$^{1,3}\Psi(A_2) = (c_1|...2a_2{}^1 3b_1{}^2 10b_2{}^2 14a_1{}^1\rangle - c_2|...2a_2{}^2 3b_1{}^1 10b_2{}^1 14a_1{}^2\rangle)(\alpha\beta \pm \beta\alpha)/\sqrt{2} \quad (1)$$

with $c_2/c_1 = 0.90$ for both the triplet and the singlet. The plus sign in eq 1 gives the spin wave function for the triplet, and the minus sign gives the spin wave function for the singlet.

Placing the unpaired $\sigma$ electron in the $14a_1$ MO and the unpaired $\pi$ electron in the $3b_1$ MO gives an electronic configuration of $B_1$ symmetry, as does placing the unpaired $\sigma$ electron in the $10b_2$ MO and the unpaired $\pi$ electron in the $2a_2$ MO. Again, these two configurations mix, but not nearly so equally as the two $A_2$ configurations. The lower-energy combination that arises from this mixing is


dx.doi.org/10.1021/ja412433t | J. Am. Chem. Soc. 2014, 136, 3589−3596

$$^{1,3}\Psi(B_1) = (c_1|...2a_2^{\,2}3b_1^{\,1}10b_2^{\,2}14a_1^{\,1}\rangle - c_2|...2a_2^{\,1}3b_1^{\,2}10b_2^{\,1}14a_1^{\,2}\rangle)(\alpha\beta \pm \beta\alpha)/\sqrt{2} \quad (2)$$

with $c_2/c_1 = 1.6$ for the triplet and 1.5 for the singlet. As in the case of the wave function in eq 1, the positive sign in the wave function in eq 2 gives the spin wave function for the triplet.

The two configurations in eqs 1 and 2 correlate the motions of the unpaired $\sigma$ and $\pi$ electrons, so that these two electrons do not simultaneously appear on the same oxygen atom. This "left−right" electron correlation is independent of the spins of the unpaired $\sigma$ and $\pi$ electrons, and this is the reason that Table 1 shows that the $^3A_2$ and $^1A_2$ electronic states are calculated to have almost exactly the same energy, as are the $^3B_1$ and $^1B_1$ electronic states.

The reason that the singlet and triplet, $B_1$, electronic states in eq 2 are calculated to have a lower energy than the singlet and triplet, $A_2$, electronic states in eq 1 is the same reason that the ratio of $c_2/c_1 = 1.6$ for the triplet and 1.5 for the singlet in eq 2 is larger than the ratio of $c_2/c_1 = 0.90$ for both the triplet and the singlet in eq 1. As shown schematically in Figure 3, the $3b_1$ and $14a_1$ MOs each have more electron density on oxygen than their $2a_2$ and $10b_2$ counterparts. Therefore, of the four electronic configurations in eqs 1 and 2, the configuration of lowest energy is the second configuration in eq 2, in which the $3b_1$ and $14a_1$ MOs are both doubly occupied.

This is, indeed, the reason that $c_2/c_1 = 1.6$ for the triplet and 1.5 for the singlet in eq 2 is larger than $c_2/c_1 = 0.90$ for both triplet and singlet in eq 1. The large coefficient in eq 2 for the lowest energy of the four configurations in eqs 1 and 2 is the reason why the singlet and triplet, $B_1$, electronic states in eq 2 are calculated to have lower energies than the singlet and triplet, $A_2$, electronic states in eq 1.

As shown in Table 1, the four electronic states of **MBQ** that are formed by loss of an electron from a $\sigma$ lone-pair orbital on oxygen in **MBQ**$^{\bullet-}$ are predicted to be responsible for the cluster of peaks in the NIPE spectrum that start at 3.75 eV. Our CASPT2 calculations predict that the $^3B_1$ peak will appear at 3.78 eV. Since this peak is for the formation of a triplet state, it should be particularly intense,[1c,17] which makes the assignment of the peak at 3.745 eV in the experimental NIPE spectrum to the formation of the $^3B_1$ state seem almost certain to be correct.

On the basis of the results of our CASPT2 calculations of the energies of the electronic states of **MBQ**, relative to the energy of the $^2A_2$ state of **MBQ**$^{\bullet-}$, we can with some confidence assign (a) peak X to the $^3B_2$ ground state, (b) peak A to the $^1B_2$ state, and (c) the peak at 3.745 eV to the $^3B_1$ state. The origin of the $^1A_1$ peak is calculated to occur at 3.62 eV; however, although the NIPE spectrum does show a peak at 3.595 eV, it is just one of several small peaks in this region. Indeed, with so many peaks in the NIPE spectrum of **MBQ**$^{\bullet-}$, it would not be very satisfactory if our calculations allowed us to make unequivocal assignments to only three of them.

**Simulations of the Vibrational Structure in the NIPE Spectra.** In order to confirm the assignments of the three bands discussed above and to assign the multitude of other peaks in the 266 nm NIPE spectrum of **MBQ**$^{\bullet-}$ in Figure 2b, we used ezSpectrum[15] to calculate Franck−Condon factors (FCFs)[16] for formation of each electronic state of **MBQ** from the $^2A_2$ state of **MBQ**$^{\bullet-}$. We then used the FCFs to simulate the vibrational structure of each band in the NIPE spectrum of **MBQ**$^{\bullet-}$.[18] A comparison between the simulated and the experimental spectra is given in Figure 4.

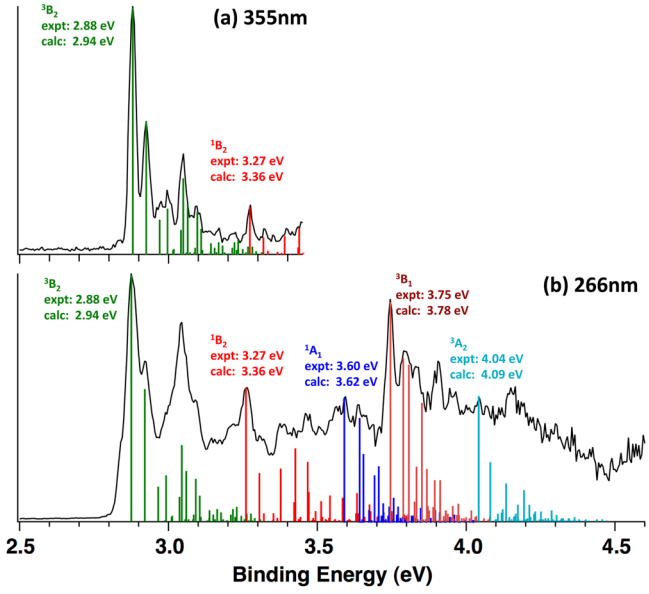


**Figure 4.** Comparison of the experimental and computed EBEs of the four lowest states of **MBQ** and the simulated NIPE spectrum, superimposed onto the experimental spectrum at (a) 355 nm and (b) 266 nm. The simulated peak positions and intensities of the 0−0 bands have been set to match those in the experimental spectra.

As shown in Figure 4, the simulated NIPE spectrum, calculated for the four, lowest-energy electronic states of **MBQ**, $^3B_2$, $^1B_2$, $^1A_1$, and $^3B_1$, provides a good fit to the experimental spectrum up to almost 4.0 eV. The peaks belonging to the $^1B_1$ electronic state are not shown in Figure 4, because as discussed above, the $^1B_1$ state has not only almost the same energy as the $^3B_1$ state but also the same orbital occupancy. Consequently, these two states have similar geometries and vibrational frequencies; thus, the vibrational peaks for formation of the $^3B_1$ and $^1B_1$ states are calculated to be very close to each other. Since the peaks for formation of the triplet are expected to have larger intensities than those for formation of the singlet,[1c,17] only the vibrational peaks that are calculated for formation of the $^3B_1$ state appear in Figure 4.

The band origin of the $^3A_2$ peak is calculated to be at an EBE of 4.09 eV. Table 1 shows that our CASPT2 calculations tend to overestimate slightly the EBEs of the band origins of the electronic states, and so we provisionally assign the peak at an EBE of 4.04 in the experimental spectrum as the $^3A_2$ band origin. However, the correspondence between the peaks in the simulated and the experimental NIPE spectra is less good for formation of states with EBEs > 4.0 eV than for formation of states with lower EBEs.

**Assignments of the Vibrational Peaks.** The good correspondence between the vibrational peaks in the first four bands of the experimental and simulated NIPE spectra of **MBQ**$^{\bullet-}$ allows us to assign the vibrational peaks in the experimental spectrum, using the identities of these peaks in the simulated spectrum. The identities of the peaks in the simulated spectrum are shown in Figure S-3 of the SI. The type of vibration that gives rise to each of these peaks is illustrated in Table S-2 in the SI, and the calculated and the observed


dx.doi.org/10.1021/ja412433t | J. Am. Chem. Soc. 2014, 136, 3589−3596

frequencies for each type of vibration in the NIPE spectrum of $\mathbf{MBQ}^{\bullet-}$ are also compared in Table S-2 in the SI.[19]

On the basis of the assignments in the SI of the vibrational peaks in the experimental NIPE spectrum of $\mathbf{MBQ}^{\bullet-}$ in Figure 4, it is possible to make some observations about the identities of these peaks. For example, the 0−0 vibrational transition from the $^2A_2$ state of $\mathbf{MBQ}^{\bullet-}$ to each of the four lowest electronic states of **MBQ** is assigned to the peak with the largest intensity within each band.

When the ground state and an excited state of a molecule have different equilibrium geometries, upon electronic excitation, progressions are seen in vibrational modes that affect the geometrical parameters that differ between the two states. For example, on removal of an electron from the $3b_1$ $\pi$ MO in the $^2A_2$ state of $\mathbf{MBQ}^{\bullet-}$, an antibonding $\pi$ interaction between C2 and both oxygens is lost. Consequently, as shown in Table 1, the C2−C1−O bond angle (and, by symmetry, the C2−C3−O bond angle) decreases by 4.5° and 4.1° in forming, respectively, the $^3B_2$ and $^1B_2$ states.

On the other hand, going from the $^2A_2$ state to the dominant configuration in the $^1A_1$ state, in which $3b_1$ is doubly occupied, one electron is removed from the $2a_2$ MO, which is antibonding between C4 (and, by symmetry, $C_6$) and O. According to Table 1, the depopulation of this MO results in the expansion of the C2−C1−O angle from 125.5° to 128.2°. The calculated decrease in this bond angle of ∼5.0° in forming the $^3B_1$, $^1B_1$, $^3A_2$, and $^1A_2$ states can be similarly rationalized.

As a result of the changes in the C2−C1−O bond angle in the $^2A_2$ state of $\mathbf{MBQ}^{\bullet-}$ upon electron loss, formation of all four of the low-lying electronic states of **MBQ** is calculated to show a progression in C2−C1−O bending that ranges from 350 to 400 $cm^{-1}$. In fact, in the experimental NIPE spectrum of $\mathbf{MBQ}^{\bullet-}$, the difference between the EBEs of the first and second peaks in the bands for the transitions to each of the low-lying states of **MBQ** is of about this size.

Of particular interest in the NIPE spectrum of $\mathbf{MBQ}^{\bullet-}$ are the C−O stretching frequencies. Unfortunately, as shown in Table 1, the C−O bond lengths in the $^2A_2$ state of $\mathbf{MBQ}^{\bullet-}$ and the $^1A_1$ state of **MBQ** are calculated to differ by only 0.017 Å. Consequently, in the NIPE spectrum of $\mathbf{MBQ}^{\bullet-}$ the band for the formation of the $^1A_1$ state of **MBQ** is calculated not to show any excitation of the C−O stretching vibrational mode.

The C−O bond lengths in the $^2A_2$ state of $\mathbf{MBQ}^{\bullet-}$ and the $^3B_2$ state of **MBQ** are calculated to differ by 0.024 Å (Table 1). Consequently, at least a weak progression in C−O stretching might be expected to be visible in the band for formation of the $^3B_2$ state. In fact, the 0−1 band in C−O stretching, coupled with C1−C6−H bending, is found by our simulation to be one of the contributors to the peak at EBE = 3.05 eV. The difference of 3.05 − 2.875 = 0.175 eV = 1410 $cm^{-1}$ between the 0−0 peak for formation of the $^3B_2$ state and the next largest peak in the region of the spectrum is only slightly smaller than the CASPT2 frequency of 1489 $cm^{-1}$ = 0.185 eV that is computed for the C−O stretching frequency in the $^3B_2$ state.

The C−O bond lengths in the $^2A_2$ state of $\mathbf{MBQ}^{\bullet-}$ and the $^1B_2$ state of **MBQ** are calculated to differ by 0.043 Å (Table 1). Consequently, a long progression in C−O stretch in the band for formation of the $^1B_2$ state of **MBQ** is predicted. Our simulation identifies the 0−1 peak in this progression as the fifth peak in the band for formation of the $^1B_2$ state. The difference between the EBE corresponding to this peak and that of the peak identified as the origin of the band for formation of the $^1B_2$ state is 3.47 − 3.265 = 0.205 eV = 1650 $cm^{-1}$, which is close to the calculated CASPT2 frequency of 1673 $cm^{-1}$ for C═O stretching in this state.

The prediction, that in the NIPE spectrum of $\mathbf{MBQ}^{\bullet-}$ the $^1B_2$ state will show a long vibrational progression in C−O stretching, whereas the $^1A_1$ will not, provides at least in principle, a way to identify which of these states is the lowest energy singlet state of **MBQ**. In fact, the simulations in Figure 4 clearly show this difference, which results in the red vibrational peaks for $^1B_2$ extending over a much wider span of EBEs than the blue vibrational peaks for the $^1A_1$ state.

Despite the complexity of the experimental NIPE spectrum, it does appear that the second group of peaks in the spectrum extends over a much wider range of EBEs than the third group. Therefore, on the basis of the relative widths of the second and third group of peaks in the experimental spectrum, the second group can be assigned to the $^1B_2$ state, and the third group, to the $^1A_1$ state. This is, of course, the energy ordering that is predicted by the results of our CASPT2/aug-cc-pVTZ//CASPT2/aug-cc-pVDZ calculations, which are given in Table 1 and in Figure 4.

## SUMMARY AND CONCLUSIONS

Well-resolved NIPE spectra of $\mathbf{MBQ}^{\bullet-}$ have been obtained at 20 K, using both 355 and 266 nm lasers for electron photodetachment. CASPT2/aug-cc-pVTZ//CASPT2/aug-cc-pVDZ single-point calculations predict accurately the positions of the 0−0 bands in the NIPE spectrum for formation of the four lowest states of **MBQ** from the $^2A_2$ state of $\mathbf{MBQ}^{\bullet-}$. In addition, the FCFs, computed from the CASPT2/aug-cc-pVDZ optimized geometries, vibrational frequencies, and normal mode vectors, successfully simulate the intensities and spacings of the vibrational peaks in the bands for formation of each of these states.

The successful simulation of the NIPE spectrum of $\mathbf{MBQ}^{\bullet-}$ allows us to make the following assignments of the electronic states of **MBQ** in the spectrum: peak X at EBE = 2.875 eV is the origin of the $^3B_2$ state; peak A at EBE = 3.265 eV is the origin of the $^1B_2$ state; peak B at EBE = 3.595 eV is the origin of the $^1A_1$ state; and peak C at EBE = 3.745 eV is the origin of the $^3B_1$ state. Thus, the NIPE spectrum and our assignments of the peaks in it confirm the two predictions, made in 1992 − the ground state of **MBQ** is a triplet ($^3B_2$), and the $^1B_2$ state is lower in energy than the $^1A_1$ state.[5a] Therefore, as predicted, although the substitution of the two oxygens in **MBQ** for the two methylene groups in **MBQDM** leaves the triplet as the ground state, this substitution reverses the ordering of the two lowest singlet states.[2c,5a]

This reversal provides the explanation for an otherwise puzzling observation. The substitution of oxygen for one methylene group of trimethylenemethane (**TMM**), to form oxyallyl (**OXA**), lowers the energy difference between the triplet and the lowest singlet state by 17.5 kcal/mol, from $\Delta E_{ST}$ = 16.2 kcal/mol in **TMM**[20] to $\Delta E_{ST}$ = −1.3 kcal/mol in **OXA**.[21] In contrast, substitution of the two oxygens in **MBQ** for the two methylene groups in **MBQDM** lowers the energy difference between the triplet and the lowest singlet state by only 0.6 kcal/mol, from $\Delta E_{ST}$ = 9.6 kcal/mol in **MBQDM**[4] to $\Delta E_{ST}$ = 9.0 kcal/mol in **MBQ**, the value that is obtained from the NIPE spectrum in Figure 4.

This apparent paradox is easily rationalized when it is realized that substitution of the two oxygens in **MBQ** for the two


dx.doi.org/10.1021/ja412433t | J. Am. Chem. Soc. 2014, 136, 3589−3596

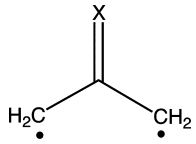


**TMM**, X = $CH_2$
**OXA**, X = O

methylene groups in **MBQDM** actually does lower the energy of the $^1B_2$ state, relative to the $^3B_2$ state, by 12.5 kcal/mol, from 21.5 kcal/mol in **MBQDM**[4] to 9.0 kcal/mol in **MBQ.** The small size of the change in the value of $\Delta E_{ST}$ on going from **MBQDM**[4] to **MBQ** is due to the fact that $^1A_1$, not $^1B_2$, is the lowest singlet state of **MBQDM.**

The reversal in the ordering of the two lowest singlet states means that, although in **MBQDM** $\Delta E_{ST}$ is the energy difference between $^1A_1$ and $^3B_2$, in **MBQ** $\Delta E_{ST}$ is the energy difference between $^1B_2$ and $^3B_2$. The energy difference between the triplet and each of these two singlet states changes dramatically on going from **MBQDM** to **MBQ.** However, the energy difference between the triplet and the lower of these two singlet states is about the same in **MBQ** as in **MBQDM**. That is why the substitution of O in **MBQ** for $CH_2$ in **MBQDM** is found, as predicted,[2c,5a] to result in a very small change (0.6 kcal/mol) in $\Delta E_{ST}$ in these two diradicals.

## ■ ASSOCIATED CONTENT

### Ⓢ Supporting Information

Geometries and absolute energies of electronic states of **MBQ**$^{\bullet-}$ and **MBQ**; simulated NIPE spectrum of **MBQDM**$^{\bullet-}$ and **MBQ**$^{\bullet-}$, showing the assignment of each vibrational peak; depictions of the observed vibrational modes, with a comparison of their calculated and observed frequencies; comparison of all of the CASPT2/aug-cc-pVDZ and (U)-B3LYP/aug-cc-pVTZ vibrational frequencies computed for **MBQ**; Mulliken atomic charges of the lowest three states in **MBQ**; and optimized geometry and energy in hartrees for each of the electronic states of **MBQ.** This material is available free of charge via the Internet at http://pubs.acs.org.

## ■ AUTHOR INFORMATION

### Corresponding Authors

xuebin.wang@pnnl.gov (X.-B.W)
borden@unt.edu (W.T.B.)

### Present Address

[#]Visiting student via PNNL Alternate Sponsored Fellowship, from State Key Laboratory of Precision Spectroscopy, East China Normal University, Shanghai 200062, China.

### Notes

The authors declare no competing financial interest.

## ■ ACKNOWLEDGMENTS

The calculations at UNT were supported by Grant CHE-0910527 from the National Science Foundation and Grant B0027 from the Robert A. Welch Foundation. The NIPES research at PNNL was supported by the U.S. Department of Energy (DOE), Office of Basic Energy Sciences, Division of Chemical Sciences, Geosciences and Biosciences (X.-B.W.), and was performed at the EMSL, a national scientific user facility sponsored by DOE's Office of Biological and Environmental Research and located at Pacific Northwest National Laboratory. We thank Professor Matthew E. Cremeens for an exchange of email messages that led to the initiation of the research described in this manuscript.

## ■ REFERENCES

(1) Borden, W. T.; Davidson, E. R. *J. Am. Chem. Soc.* **1977**, *99*, 4587. Reviews: (b) Borden, W. T. In *Diradicals*; Borden, W. T., Ed,; Wiley: New York, 1982; pp 1−72. (c) Lineberger, W. C.; Borden, W. T. *Phys. Chem. Chem. Phys.* **2011**, *13*, 11792.

(2) Kato, S.; Morokuma, K.; Feller, D.; Davidson, E. R.; Borden, W. T. *J. Am. Chem. Soc.* **1983**, *105*, 1791. (b) Lahti, P. M.; Rossi, A. R.; Berson, J. A. *J. Am. Chem. Soc.* **1985**, *107*, 2273. (c) Hrovat, D. A.; Murcko, M. A.; Lahti, P. M.; Borden, W. T. *J. Chem. Soc., Perkin Trans. 2* **1998**, 1037.

(3) Wright, B. B.; Platz, M. *J. Am. Chem. Soc.* **1983**, *105*, 628.

(4) Wenthold, P. G.; Kim, J. B.; Lineberger, W. C. *J. Am. Chem. Soc.* **1997**, *119*, 1354.

(5) (a) Fort, R. C., Jr.; Getty, S. J.; Hrovat, D. A.; Lahti, P. M.; Borden, W. T. *J. Am. Chem. Soc.* **1992**, *114*, 7549. (b) Morales-Roque, J.; Carrillo-Cárdenas, M.; Jayanthi, N.; Cruz, J.; Pandiyan, T. *J. Mol. Struct. (THEOCHEM)* **2009**, 74. (c) Altarawneh, M.; Dlugogorski, B. Z.; Kennedy, E. M.; Mackie, J. C. *J. Phys. Chem. A* **2010**, *114*, 1098.

(6) Reviews: (a) Platz, M. In *Diradicals*; Borden, W. T., Ed.; Wiley: New York, 1988; pp 195−258. (b) Berson, J. A. In *The Chemistry of Functional Groups-Quinones*; Patai, S., Ed.; Wiley: New York, 1988; Vol. 2, p 455.

(7) Fattahi, A.; Kass, S. R.; Liebman, J. F.; Matros, M. A. R.; Miranda, M. S.; Morais, V. M. F. *J. Am. Chem. Soc.* **2005**, *127*, 6116. (b) Roithová, J.; Schröder, D.; Schwarz, H. *Chem.—Eur. J.* **2005**, *11*, 628. (c) Wenthold, P. G. *J. Am. Soc. Mass Spectrom.* **2007**, *18*, 2014.

(8) Fu, Q.; Yang, J.; Wang, X.-B. *J. Phys. Chem. A* **2011**, *115*, 3201.

(9) Wang, X. B.; Wang, L. S. *Rev. Sci. Instrum.* **2008**, *79*, 073108.

(10) Dunning, T. H., Jr. *J. Chem. Phys.* **1989**, *90*, 1007. (b) Kendall, R. A.; Dunning, T. H., Jr.; Harrison, R. J. *J. Chem. Phys.* **1992**, *96*, 6769.

(11) Borden, W. T.; Davidson, E. R. *Acc. Chem. Res.* **1996**, *29*, 87.

(12) Andersson, K.; Malmqvist, P.-Å.; Roos, B. O. *J. Chem. Phys.* **1992**, *96*, 1218.

(13) Andersson, K.; Aquilante, F.; Barysz, M.; Bernhardsson, A.; Blomberg, M. R. A.; Carissan, Y.; Cooper, D. L.; Cossi, M.; DeVico, L.; Ferré, N.; Fülscher, M. P.; Gaenko, A.; Gagliardi, L.; Ghigo, G.; de Graaf, C.; Gusarov, S.; Hess, B. A.; Hagberg, D.; Holt, A.; Karlström, G.; Lindh, R.; Malmqvist, P.-Å.; Nakajima, T.; Neogrády, P.; Olsen, J.; Pedersen, T.; Pitonak, M.; Raab, J.; Reiher, M.; Roos, B. O.; Ryde, U.; Schimmelpfennig, B.; Schütz, M.; Seijo, L.; Serrano-Andrés, L.; Siegbahn, P. E. M.; Stålring, J.; Thorsteinsson, T.; Veryazov, V.; Widmark. P.-O. *MOLCAS* version 7, Lund University: Sweden, 2008.

(14) For calculations on **MBQ**$^{\bullet-}$ and on the three lowest electronic states of **MBQ**, in which the nonbonding 2p−$\sigma$ AOs on both oxygens remain doubly occupied, including this pair of AOs and the electrons in them in the active space, proved to be unimportant. When (12/10) CASSCF calculations on these electronic states were begun with these oxygen 2p−$\sigma$ AOs and the electrons in them placed in the active space, other $\sigma$ orbitals were found to replace these oxygen AOs in the converged (12/10)CASSCF wave functions.

(15) Mozhayskiy, V. A.; Krylov, A. I. *ezSpectrum*, version 3.0; see http://iopenshell.usc.edu/downloads.

(16) (a) Frank, J. *Trans. Faraday Soc.* **1926**, *21*, 536. (b) Condon, E. *Phys. Rev.* **1926**, *28*, 1182.

(17) Clifford, E. P.; Wenthold, P. G.; Lineberger, W. C.; Ellison, G. B.; Wang, C. X.; Grabowski, J. J.; Vila, F.; Jordan, K. D. *J. Chem. Soc., Perkin Trans. 2* **1998**, 1015.

(18) We also simulated the NIPE spectrum of **MBQDM**$^{\bullet-}$ using the CASPT2/aug-cc-pVDZ optimized geometries, frequencies, and normal mode vectors; and the CASPT2/aug-cc-pVTZ electron binding energies. The simulated NIPE spectrum of **MBQDM**$^{\bullet-}$ is shown in Figure S-1 of the SI, where it is compared with the experimental spectrum, obtained by Wenthold, Kim, and Lineberger.[4] The good agreement between the simulated and experimental NIPE spectra of **MBQDM**$^{\bullet-}$ in Figure S-1 of the SI gives us confidence that the similarly good agreement between the simulated and experimental

NIPE spectrum of **MBQ**$^{\bullet-}$ in Figure 4 is not accidental and that our computational methodology is reliable.

(19) Also available in the SI in Table S-3 is a comparison of the CASPT2/aug-cc-pVDZ vibrational frequencies, calculated from finite energy differences, with the (U)B3LYP/aug-cc-pVTZ vibrational frequencies, calculated using analytical second derivatives of the energies.

(20) (a) Wenthold, P. G.; Hu, J.; Squires, R. R.; Lineberger, W. C. *J. Am. Chem. Soc.* **1996**, *118*, 475. (b) Wenthold, P. G.; Hu, J.; Squires, R. R.; Lineberger, W. C *J. Am. Soc. Mass Spectrom.* **1999**, *10*, 800.

(21) (a) Ichino, T.; Villano, S. M.; Gianola, A. J.; Goebbert, D. J.; Velarde, L.; Sanov, A.; Blanksby, S. J.; Zhou, X.; Hrovat, D. A.; Borden, W. T.; Lineberger, W. C. *Angew. Chem., Int. Ed.* **2009**, *48*, 8509. (b) Ichino, T.; Villano, S. M.; Gianola, A. J.; Goebbert, D. J.; Velarde, L.; Sanov, A.; Blanksby, S. J.; Zhou, X.; Hrovat, D. A.; Borden, W. T.; Lineberger, W. C. *J. Phys. Chem. A* **2011**, *115*, 1634.